

Bacteriophage Twort protein Gp168 is a β -clamp inhibitor by occupying the DNA sliding channel

Bing Liu^{1,2,*}, Shanshan Li^{3,†}, Yang Liu^{1,†}, Huan Chen¹, Zhenyue Hu¹, Zhihao Wang^{1,2}, Yimin Zhao⁴, Lei Zhang⁴, Biyun Ma¹, Hongliang Wang⁵, Steve Matthews², Yawen Wang^{1,*} and Kaiming Zhang^{3,*}

¹BioBank, The First Affiliated Hospital of Xi'an Jiaotong University, Shaanxi 710061, China, ²Department of Life Sciences, Faculty of Natural Sciences, Imperial College London, London SW7 2AZ, United Kingdom, ³MOE Key Laboratory for Membraneless Organelles and Cellular Dynamics, Hefei National Laboratory for Physical Sciences at the Microscale and Division of Life Sciences and Medicine, University of Science and Technology of China, Hefei 230027, China, ⁴MOE Key Laboratory for Nonequilibrium Synthesis and Modulation of Condensed Matter, School of Physics, Xi'an Jiaotong University, Xi'an 710049, China and ⁵Department of Pathogen Biology and Immunology, Xi'an Jiaotong University Health Science Center, Xi'an, Shaanxi 710061, China

Received May 24, 2021; Revised September 13, 2021; Editorial Decision September 14, 2021; Accepted September 16, 2021

ABSTRACT

Bacterial chromosome replication is mainly catalyzed by DNA polymerase III, whose beta subunits enable rapid processive DNA replication. Enabled by the clamp-loading complex, the two beta subunits form a ring-like clamp around DNA and keep the polymerase sliding along. Given the essential role of β -clamp, its inhibitors have been explored for antibacterial purposes. Similarly, β -clamp is an ideal target for bacteriophages to shut off host DNA synthesis during host takeover. The Gp168 protein of phage Twort is such an example, which binds to the β -clamp of *Staphylococcus aureus* and prevents it from loading onto DNA causing replication arrest. Here, we report a cryo-EM structure of the clamp–Gp168 complex at 3.2-Å resolution. In the structure of the complex, the Gp168 dimer occupies the DNA sliding channel of β -clamp and blocks its loading onto DNA, which represents a new inhibitory mechanism against β -clamp function. Interestingly, the key residues responsible for this interaction on the β -clamp are well conserved among bacteria. We therefore demonstrate that Gp168 is potentially a cross-species β -clamp inhibitor, as it forms complex with the *Bacillus subtilis* β -clamp. Our findings reveal an alternative mechanism for bacteriophages to inhibit β -clamp and provide a new strategy to combat bacterial drug resistance.

INTRODUCTION

DNA replication is a polymerization process that includes three coordinated steps: initiation, elongation, and termination (1). In bacteria, the elongation process is mediated by the DNA polymerase (Pol) III core enzyme and beta subunits (β -clamp or sliding clamp). During elongation, the β -clamp allows DNA Pol III to slide along DNA by forming a ring-like structure with two subunits that completely encircle double-stranded DNA (dsDNA) (2). The process of β -clamp loading on DNA is assisted by the clamp loader of DNA Pol III, comprises seven subunits (δ , 3τ or γ , δ' , χ and ψ) in *E. coli* (3,4). While subunit τ is not essential for clamp loading, it does contribute to the formation of DNA Pol III holoenzyme (5). Since the β -clamp/core DNA Pol interaction allows the complex to slide freely along dsDNA, which greatly improves the processivity of polymerase, thereby increasing the rate of DNA synthesis (6). Bacterial β -clamp is dimeric with each monomeric unit consisting of three domains. Its counterparts are highly conserved among archaea, eukaryotes, and viruses (7–10), despite differences in their sequences and multimeric states (11).

Besides its role in processive DNA replication, β -clamp also participates in other important cellular events by interacting with other proteins, including other DNA polymerases, DNA ligases, MutS and MutL (12). Interestingly, all of these proteins interact with β -clamp through the hydrophobic protein-binding pocket located on the surface of its ring (13). In contrast, the DNA duplex passes through the charged channel formed by the two clamp subunits, perpendicular to the plane of the ring and distal from the

*To whom correspondence should be addressed. Tel: +86 02985324475; Fax: +86 02985324474; Email: bliu@imperial.ac.uk

Correspondence may also be addressed to Yawen Wang. Email: wangyawen@xjtu.edu.cn

Correspondence may also be addressed to Kaiming Zhang. Email: kmzhang@ustc.edu.cn

[†]The authors wish it to be known that, in their opinion, the first three authors should be regarded as Joint First Authors.

protein-binding pocket (14). Notably, there is no interactor protein that engages the inner circle of the β -clamp ring (the DNA binding channel) other than DNA to our knowledge.

Bacteriophages have developed strategies to suppress host DNA replication to scavenge all available resources for their progeny production. Phage Twort and G1 of Gram-positive *Staphylococcus aureus* were reported to produce β -clamp inhibitors Gp168 and Gp240, respectively (15). Importantly, the impairment of host DNA synthesis by Gp168 and Gp240 can be observed in two separate events, namely the β -clamp loading step and the processive DNA synthesis after the clamp-loading, which highlights the potent inhibitory effect of these phage proteins (16). Stepwise reconstitution of processive DNA replication *in vitro* showed that 100-fold excess of δ subunit of the clamp loader and DNA Pol III were required to displace the phage proteins from β -clamp at clamp-loading step, and the phage proteins caused up to 70% inhibition of DNA synthesis after β -clamp loading on DNA. Therefore, Gp168 and Gp240 were proposed to engage the β -clamp via a binding site that overlaps with that of δ and PolC on the clamp, i.e. the hydrophobic protein-binding pocket.

Here, we report detailed structural and biophysical studies of the clamp inhibitor Gp168 from phage Twort. We demonstrate that Gp168 exists as a hexamer free in the solution, while it adopts a dimeric form in a complex with β -clamp, suggesting that the disassembly of the Gp168 hexamer occurs during the formation of the Gp168-clamp complex. Notably, Gp168 does not occupy the hydrophobic protein-binding pocket of the β -clamp but occupies the DNA sliding channel of β -clamp where it blocks DNA loading, revealing a new mode of clamp-inhibition. Furthermore, we identify the key residues responsible for the complex formation and demonstrate that Gp168 interacts with *Bacillus subtilis* β -clamp beyond its native host due to cross-species conservation. Therefore, our findings reveal a novel strategy employed by bacteriophages to inhibit the host DNA synthesis, a new protein-binding site on β -clamp, and a potential new drug target site for screening anti-bacterial compounds.

MATERIALS AND METHODS

Protein expression

Gp168 gene was chemically synthesized and PCR amplified, while β -clamp genes were directly amplified from bacterial genomes. The PCR product was purified and cloned into the pDE1 vector with an N-terminal polyhistidine-tag and transformed into the *E. coli* strain BL21 (DE3) for expression of the recombinant fusion protein. The recombinant strain was grown in LB media and 50 μ g/ml kanamycin at 37°C. When the recombinant strain culture was grown to mid-log phase ($OD_{600} = 0.6-0.8$), it was induced by 1 mM IPTG and harvested after 3-h incubation at 37°C. The bacterial pellet was collected by centrifugation at 5000 rpm, at 4°C for 10 min and then resuspended in binding buffer (300 mM NaCl, 50 mM Na₂HPO₄, 10 mM imidazole, pH8.0). The lysis of the cells was achieved via sonication and centrifuged at 17 000g at 4°C for 30 min and the supernatant was subjected to standard polyhistidine-tag purification under native condition using Ni-NTA (Qiagen).

The purified Gp168 fraction was dialyzed in the dialysis buffer (250 mM NaCl, 50 mM Na₂HPO₄, 0.2 mM TCEP, pH8.0) at 4°C overnight and concentrated by ultrafiltration with a 10 kDa cut-off filter 3 h to 2 ml for subsequent experiments. The fusion protein was further purified using HiLoad Superdex 75 pg or 200 pg column (GE healthcare).

Pull-down experiment

The β -clamp genes of *S. aureus* and *B. subtilis* were PCR amplified from their genomic DNA, respectively. The PCR products were purified and cloned into a modified pET-46 vector without any N-terminal tag, and the recombinant tagless proteins were expressed as described above. The polyhistidine-tag Gp168 or Gp168 mutants that purified from 0.5 liter of recombinant strain culture were preloaded into the Ni-NTA column and equilibrated with a binding buffer containing 300 mM NaCl, 50 mM sodium phosphate, 10 mM Imidazole, and 0.5 mM TCEP at pH 8.0. Two liters of β -clamp or its mutants overexpressing cell culture were harvested and the cell pellet was resuspended in 30 ml binding buffer, which was subjected to sonication and centrifugation as described above. After centrifugation, the supernatant was added to the Gp168 preloaded column to perform pull-down experiments. The column was first washed 4 column volumes of binding buffer, and subsequently 10 column volumes of washing buffer (300 mM NaCl, 50 mM Na₂HPO₄, 20 mM imidazole, pH8.0) and 2 column volumes of elution buffer (300 mM NaCl, 50 mM Na₂HPO₄, 250 mM imidazole, pH 8.0). The final elute was concentrated by ultrafiltration and analyzed using HiLoad 200 pg column. Each pull-down assay was performed three times and the reported data were based three consistent results.

For pull-down experiments performed using cell lysate of *B. subtilis*, *B. subtilis* strain 168 (ATCC No. 23857) was used. Four liters of *B. subtilis* culture were harvested at $OD_{600} \sim 1.2$ by centrifugation at 5000 rpm, at 4°C for 10 min and resuspended in 100 ml of the binding buffer. The rest of the experiment followed the steps described above using β -clamp overexpressing *E. coli* culture. The pull-down assay was performed three times and the reported data were based on three consistent results.

Size exclusion chromatography

Proteins were further purified and analyzed using an automated Äkta pure system in relevant dialysis buffers. Based on the molecular weights and the multimeric states of the proteins, the corresponding HiLoad column was selected. The Superdex 75 pg column was used for purification and assessment of the multimeric state for Gp168 and the Superdex 200 pg column was for testing the complex formation. Both columns were calibrated using low molecular weight Gel filtration marker kit (12 000 to 200 000 Da, Sigma) and elution profiles of the calibration kit proteins are shown in Supplementary Figure S1.

NMR spectroscopy

All NMR experiments were recorded on a Bruker 600 MHz (Avance III) spectrometer at 298 K with 128 scans. The

sample was in a buffer containing 50 mM NaH₂PO₄, 300 mM NaCl (pH 7.0) at 300 K.

ITC

ITC experiments were performed on a MicroCal PEAQ-ITC Instrument (Microcal) at 25°C using the dialysis buffer described above. β-Clamp of 60 μM in the cell was titrated with 1 mM Gp168 in the syringe via 19 injections with 2 μl each at 120 s interval. The raw data were integrated, normalized for the molar concentration and analyzed using MicroCal PEAQ-ITC Analysis Software.

SEC-MALS

A total of 100 μl protein sample (500 μM) was injected at 0.2 ml/min to a Superdex 75 10/300 GL size-exclusion column (GE Healthcare) that was connected to the Agilent HPLC 1100 (including degasser, pump, and UV detector) in line with a multi-angle laser light (690 nm) scattering detector (miniDAWN TREOS, Wyatt Technology, Santa Barbara, CA) and a relative refractive interferometer (Optilab T-REX refractometer, Wyatt Technology, Santa Barbara, CA). The experiment was performed at 25°C. ASTRA 6.1 software was used for data collection and analysis, and the solvent refractive index was defined as 1.331, the solvent viscosity was defined as 0.8945 cP, and the refractive index increment value (dn/dc) was defined as 0.185 ml/g.

Cryo-EM data acquisition

The sample was diluted at a final concentration of around 0.3 mg/ml. Three microliters of the samples were applied onto glow-discharged 200-mesh R2/1 Quantifoil copper grids. The grids were blotted for 4 s and rapidly cryocooled in liquid ethane using a Vitrobot Mark IV (Thermo Fisher Scientific) at 4°C and 100% humidity. The samples were imaged in a Titan Krios cryo-electron microscope (Thermo Fisher Scientific) operated at 300 kV with a GIF energy filter (Gatan) at a magnification of 105 000× (corresponding to a calibrated sampling of 0.82 Å per pixel). Micrographs were recorded by EPU software (Thermo Fisher Scientific) with a Gatan K3 Summit direct electron detector, where each image was composed of 30 individual frames with an exposure time of 2.5 s and an exposure rate of 22.3 electrons per second per Å². A total of 7739 movie stacks were collected.

Single-particle image processing and 3D reconstruction

All micrographs were first imported into Relion (17) for image processing. The motion-correction was performed using MotionCor2 (18) and the contrast transfer function (CTF) was determined using CTFFIND4 (19). Then the micrographs with 'rlnCtfMaxResolution < 5' were selected using the 'subset selection' option in Relion. All particles were autopicked using the NeuralNet option in EMAN2. Then, particle coordinates were imported to Relion, where the poor 2D class averages were removed by several rounds of 2D classification. Initial maps were built and classified using ab-initio 3D reconstruction in cryoSPARC (20) without any symmetry applied. Two good classes having 507 603

particles were selected and subjected to the 3D heterogeneous refinement to remove junk 3D classes. One good class containing 218 035 particles was selected and then the non-uniform refinement combined with the local/global CTF refinement was performed with C2 symmetry applied, and a 3.2-Å resolution map was obtained. Resolution for the final map was estimated with the 0.143 criterion of the Fourier shell correlation curve. Resolution map was calculated in cryoSPARC using the 'Local Resolution Estimation' option. The figures were prepared using UCSF Chimera (21) (More information in Supplementary Figure S2 and Supplementary Table S1).

Model building

The 3.2-Å cryo-EM map was first computationally segmented (22). The β-clamp was first modeled using SWISS-MODEL and fitted to the computationally extracted β-clamp monomer map. The resultant model was refined using phenix.real_space_refine (23) and manually optimized with Coot (24). Phenix.map_to_model (25) was used to generate the initial model of Gp168 fitted into the computationally extracted Gp168 monomer map. Coot was then used to confirm the amino acid sequence registration of the initial model and assign amino acids to the cryo-EM density regions that were not resolved by phenix.map_to_model. Then an atomic model composed of residues 12–54 was obtained. The atomic models of the β-clamp and Gp168 protomer were combined and subjected to phenix.real_space_refine. The resultant model was then fitted into the cryo-EM density of the other protomers using Chimera, followed by the optimization of the whole model with phenix.real_space_refine. The final model was evaluated by MolProbity and Q-scores. Statistics of the map reconstruction and model optimization are shown in Supplementary Table S1. All figures were prepared using Chimera.

Mutagenesis

Site-directed mutagenesis was performed with back-to-back PCR amplification using forward primers bearing the mutation to introduce. The primers were designed by NEB online design software, NEBaseChanger. The primers used in mutagenesis are listed in Supplementary Table S2.

RESULTS

Gp168 exists as a hexameric complex in solution

To evaluate how *S. aureus* phage proteins directly engage β-clamp *in vitro*, we focused on Gp168 from a previous study (16). After purification of recombinant polyhistidine-tagged Gp168 (His-Gp168), we first characterized its biophysical property in solution. Although the recombinant protein appeared at the expected molecular weight in SDS-PAGE, we noted that the elution volume of Gp168 in the gel filtration was much larger than that expected for a monomer and corresponded to a much larger protein (Figure 1A). Structural analysis by ¹H NMR spectroscopy showed that the protein was folded and existed as a high-order multimer as the peak line-widths were much broader than expected for a small protein. It is also noteworthy that the spectrum

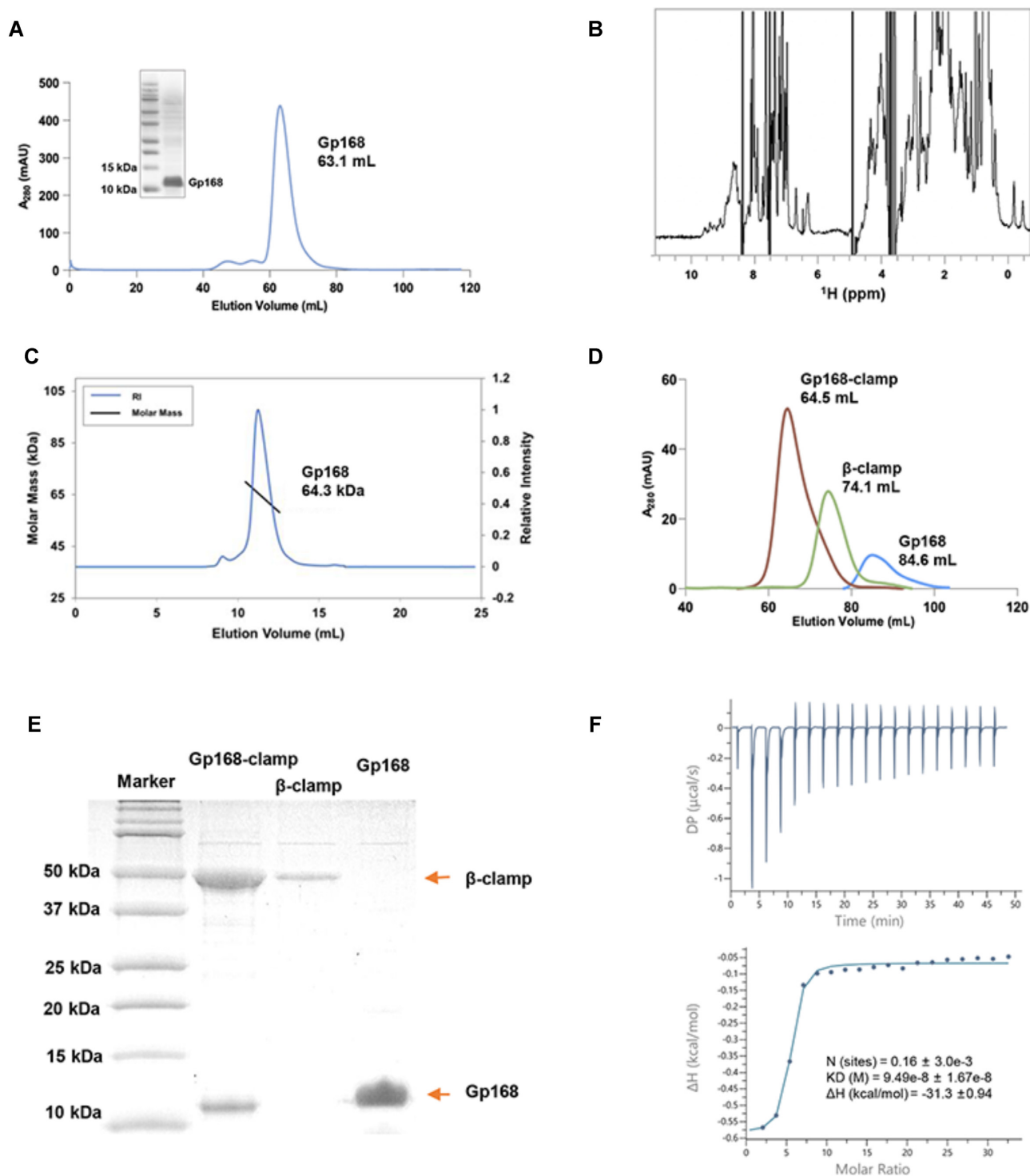


Figure 1. Gp168 exists as a hexamer in solution and forms a stable complex with β -clamp. (A) SDS-PAGE image and gel filtration chromatographic profile of the Gp168 sample. The chromatography was performed using a Hiload Superdex 75 column. (B) 1D ^1H NMR spectrum of Gp168 recorded in 50 mM NaH_2PO_4 , 300 mM NaCl (pH 7.0) at 300 K. (C) Absolute molar mass of Gp168 in the buffer stated in (B) was determined at 64.3 kDa by SEC-MALS. (D) Gel filtration chromatographic profiles of β -clamp (green), Gp168 (blue) and Gp168-clamp complex (brown). The chromatography was performed using a Hiload Superdex 200 column. (E) SDS-PAGE of the corresponding fractions from (D). (F) ITC results for β -clamp and Gp168. The K_D value for the interaction was calculated to be 95 nM.

lacks H α signals above 5 ppm characteristic of beta-strand secondary structure (Figure 1B). To determine the multi-meric state of Gp168 in solution, multi-angle light scattering coupled with size-exclusion chromatography (SEC-MALS) was applied, and a calculated MW of 64.3 kDa was derived (Figure 1C). As the MW of His-tagged Gp168 monomer is 10.6 kDa, Gp168 is likely to be hexameric in solution.

Gp168 forms a stable complex with β -clamp

We next performed the pull-down assay using purified His-tagged Gp168 and cell lysate of *E. coli*, where untagged *S. aureus* β -clamp was over-expressed. We observed that the His-tagged Gp168 co-eluted with the untagged β -clamp and consequently verified complex formation by gel filtration chromatography (Figure 1D and E). The gel filtration profile shows that the interaction between Gp168 and β -clamp is maintained throughout the elution (Figure 1D). Moreover, the binding affinity (K_D) calculated using Isothermal Titration Calorimetry (ITC) was estimated to be 95 ± 16.7 nM (Figure 1F), which is significantly stronger than the interaction between β -clamp and DNA (14). Since β -clamp has a six-domain ring-like structure, we expected that the hexameric Gp168 would engage the six-domain β -clamp to form a head-to-head complex containing six Gp168 molecules and two β subunits, with a combined MW of 150 kDa. However, although the Gp168-clamp complex had a larger MW than either Gp168 hexamer or β -clamp dimer, its MW was estimated at 100 kDa based on the elution volume and was significantly smaller than that expected for a 6:2 complex (Figure 1D). Therefore, Gp168 forms a stable complex with β -clamp in a different stoichiometry.

Cryo-EM single-particle analysis of the Gp168-clamp complex

To further understand the formation of the Gp168-clamp complex, we performed cryogenic electron microscopy (cryo-EM) single-particle analysis of this complex obtained from size-exclusion chromatography. The sample produced optimal grids at a concentration of ~ 0.3 mg/ml. The raw images revealed that the molecules occupied 60–80% of the raw image area in multiple orientations (Figure 2A), which was deemed to be suitable for 3D reconstruction. A total of $\sim 1\,630\,000$ particles out of 7739 movie images were selected and subjected to reference-free 2D classification (Figure 2B and Supplementary Figure S2A). The 2D class averages showed that the complex adopted the annulus shape, akin to the β -clamp structure and was consistent with the previous study (14). Notably, extra density was observed in the center of the annulus and could be attributed to the bound Gp168 (Figure 2B). Final 3D refinement was conducted with and without C2 symmetry to obtain 3.2- and 3.4-Å maps, respectively, which had a high cross-correlation coefficient ($CC = 0.98$) (Supplementary Figure S2A and S2B). Hereafter, we analyzed the structural details of the 3.2-Å symmetric map which displayed adequate orientation sampling (Supplementary Figure S2C). In accordance with the 2D class averaging analy-

sis, the 3.2-Å final map showed that the Gp168-clamp complex had a six-domain ring structure with Gp168 located within the ring center (Figure 2C and Supplementary Figure S2D). The local resolution varied in the map, and the densities at the bottom of the center region had a lower resolution compared with other regions (Supplementary Figure S2E), likely resulting from the inherent flexibilities of the N- and C-termini of Gp168.

To illustrate the structural details of Gp168 and its interactions with β -clamp, we *de novo* built the atomic model of Gp168 bound to β -clamp. The cryo-densities of the secondary structure elements and the majority of the side chains were clearly visible and consistent with the amino acid sequences, which was especially important for Gp168 (Figure 2D) as its structure had not been resolved before. We validated the resultant complete model using MolProbity (26) (Supplementary Table S1). The Q -scores developed for evaluating the density resolvability (27) were further conducted to validate the quality of the Gp168 structure. The reliability of the structure was supported by the fact that the Q -scores for the entire structure of this small protein were comparable to the expected Q -scores at the same resolution resulting from cryo-EM analysis (Figure 2E).

Gp168 is a new class of β -clamp inhibitor that does not mimic DNA

In the structure of the Gp168-clamp complex, Gp168 consisting of two anti-parallel helices existed in the form of a dimer that occupied the DNA sliding channel of β -clamp (Figure 3A) and the interaction between the second α -helix of chain A ($G\alpha^2$) and that of chain B ($G\beta^2$) was crucial for the dimer formation (Figure 3B). The PDBsum structure bioinformatics software (28) indicates that the dimer interface occupies about 800 \AA^2 and involves two salt bridges formed between K20-E48, four hydrogen bonds formed between K20-E48, Y47-E48, and multiple non-bonded contacts to form a stable dimer interface. Meanwhile, the contact points between Gp168 and β -clamp were confined to the first α -helices of each chain in Gp168 ($G\alpha^1$ and $G\beta^1$) and the domain IIIs of the clamp, which is reminiscent of the DNA-clamp interaction rather than other protein-clamp interactions (Figure 3A). This is distinct from previously described protein-clamp interactions (12,29,30), in which proteins, such as the clamp loader and PolC, occupy the protein-binding pocket located between domain II and domain III of the clamp. Therefore, we postulated that Gp168 was a DNA mimic protein that can compete with DNA for β -clamp binding (14).

Although the Gp168 homodimer displays an overall negatively charged surface that is located on the front and back of the structure as shown in Figure 3C (left), this arrangement does not resemble the precise surface charge distribution of dsDNA (Figure 3D). In contrast, the clamp interacting surface of Gp168 was distinct from these negatively charged surfaces. In particular, Y14 extends away from the structure and its sidechain contacts domain III of the β -clamp, indicating a potential role in the interaction. We then built the *S. aureus* DNA-clamp complex by superimposing our structure with the previous published

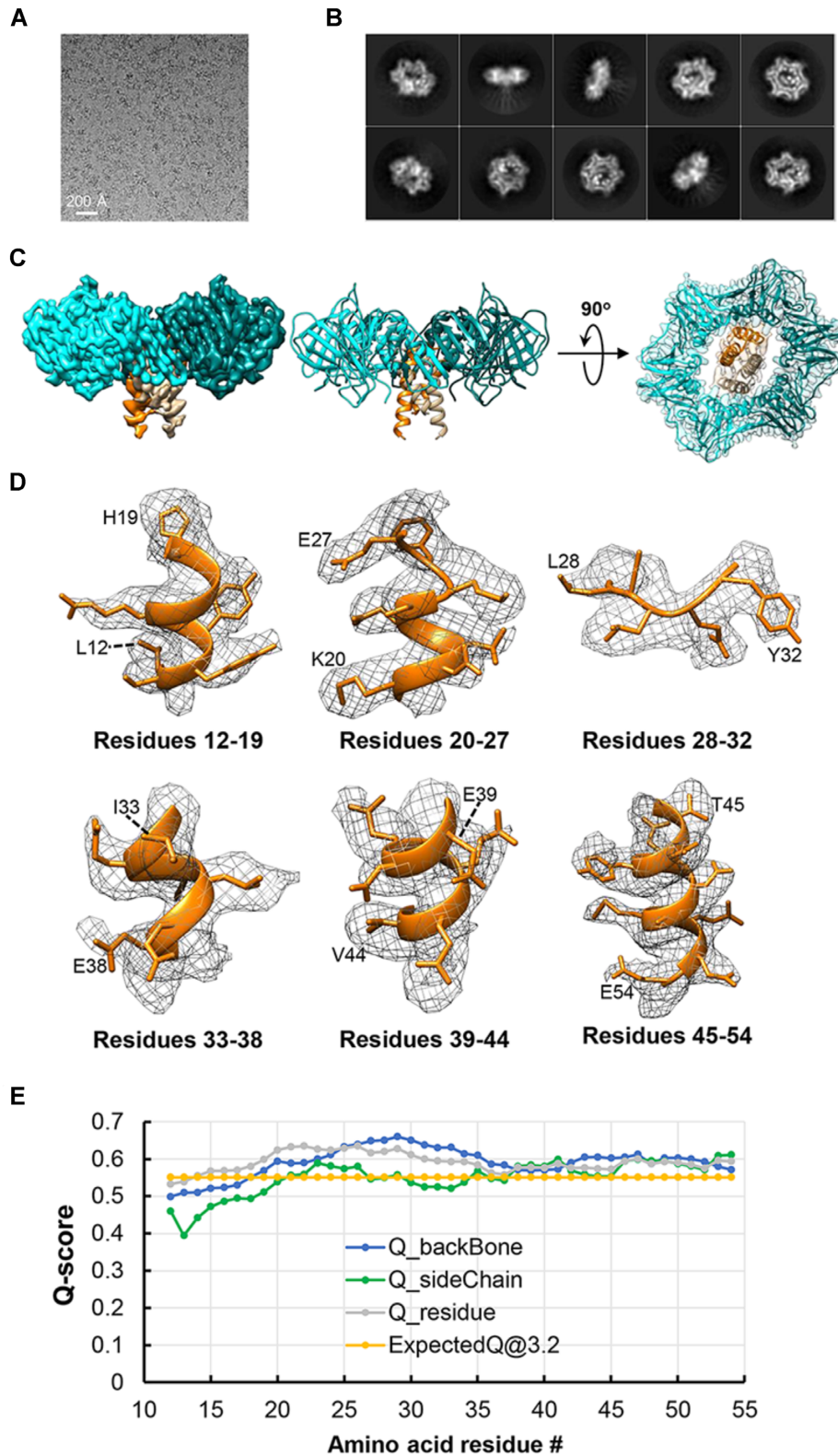


Figure 2. Cryo-EM single-particle analysis of the Gp168-clamp complex. (A) Representative motion-corrected cryo-EM micrograph. (B) Reference-free 2D class averages. (C) The 3.2-Å cryo-EM map and model of the β -clamp (cyan and teal) bound with Gp168 (orange and wheat). (D) Gp168 protomer fitted into its zoned map, which was divided into six portions to better display the residue sidechain and prove its good resolvability. (E) Q -score for each residue in the model and 3.2-Å zoned map of gp168; the gold dotted line represents the expected Q -score at 3.2-Å resolution (0.5512) based on the correlation between Q -scores and map resolution.

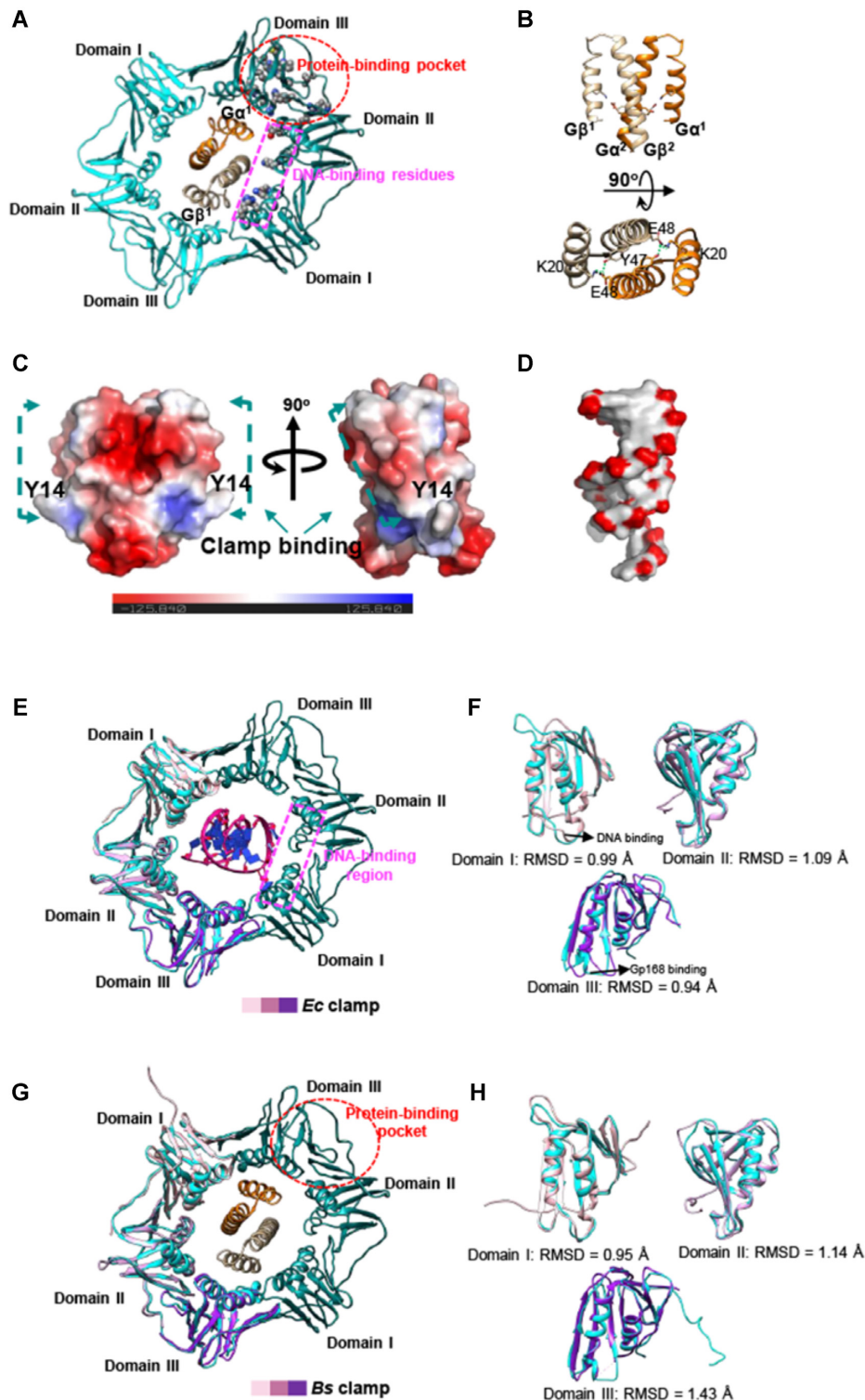


Figure 3. Structural features of Gp168 and *S. aureus* β -clamp. (A) Overall structure of the Gp168-clamp complex with individual domains of β -clamp and chains of Gp168 labeled. β -clamp is displayed in cyan and teal to illustrate two subunits and Gp168 is displayed in orange and wheat to illustrate two chains. The sidechain atoms of key residues in the protein binding pocket (circled in red) and the DNA binding residues (in purple rectangle) are colored by element: C (grey), N (blue), O (red) and S (Yellow). (B) Structural characteristics of the Gp168 homodimer with helices in each chain labeled. Two salt bridges were formed between K20-E48 (black dash line) and four hydrogen bonds were formed between K20-E48, Y47-E48 (green dash line). (C) The electrostatic surface of the dimer shown in the same orientation as in (B) with Y14 highlighted. (D) The negatively charged phosphate backbone of dsDNA. (E) An *S. aureus* DNA-clamp complex model by superimposing our structure with the previous published *E. coli* complex (PDB ID: 3BEP). (F) The comparison of corresponding domains between *S. aureus* and *E. coli* β -clamps, with the DNA binding loop and Gp168 binding loop indicated. (G) An *B. subtilis* gp168-clamp complex model by superimposing our structure with the previous published *B. subtilis* complex (PDB ID: 6E8D). (H) The comparison of corresponding domains between *S. aureus* and *B. subtilis* β -clamps.

E. coli complex (PDB ID: 3BEP) (14) to examine the similarity between Gp168 and dsDNA in their clamp interactions (Figure 3E). Indeed, Gp168 was not in direct contact with key residues responsible for DNA binding (Figure 3A, E and Supplementary Figure S3A). The above result suggests that although Gp168 is not an exact mimic of DNA, it is able to inhibit DNA binding by occupying the DNA sliding channel of β -clamp. Notably, *S. aureus*, *E. coli* and *B. subtilis* (PDB ID: 6E8D) (30) β -clamps possess a high structural conservation, as demonstrated by a low RMSD calculated between corresponding domains (Figure 3E–H). Some conformational differences are observed in the Gp168- and DNA-binding regions between *S. aureus* and *E. coli* β -clamps, respectively (Figure 3E and F). And the protein-binding pocket the Sa_clamp-Gp168 complex remains largely undisturbed when compared with the structure of the most closely related β -clamp available (Bs_clamp, and Figure 3G and H).

The pairwise alignment of Gp168 and Gp240 suggests that they would adopt a similar fold with a shared 46% sequence identity (Supplementary Figure S3B). Thus, we built the Gp240 structure model by homology modeling (31) using our resolved Gp168 structure as the template. The homology model of Gp240 (residue 16–54) reveals that most residues in contact with β -clamp are identical, but the helices responsible for Gp240 dimerization are shorter (Supplementary Figure S3B and C). To identify other potential Gp168-like clamp inhibitors, we performed sequence and structural homology search (32,33). The sequence comparison did not retrieve any sequence homolog even in other phages, and the structural search showed that Gp168 had no significant similarity to other protein structures. There was a degree of resemblance to the *de novo* designed protein homo-oligomers (PDB ID: 5IZS) (34). Therefore, Gp168 and Gp240 likely represent a new class of proteins with other members yet to be discovered.

Residues critical for Gp168–clamp interactions

To further understand how Gp168 inhibits β -clamp, we analyzed the interactions between Gp168 and β -clamp using PDBsum (28). The Gp168-clamp interface was approximately 443 Å² and involved multiple non-bonded contacts. Hydrogen bonds are formed between the sidechain hydroxyl of Y14_{Gp168} and the backbone of E284-G285_{clamp}, and between sidechains of D21_{Gp168} and N288_{clamp}. Hydrophobic contacts are present between M25_{Gp168} and the aliphatic portion of K333_{clamp} and R283_{clamp} sidechains, and L30_{Gp168} with M334_{clamp} and D336_{clamp} (Figure 4A). Furthermore, the flanking negatively charge surfaces on the Gp168 dimer complement the positively charged inner surface of the β -clamp (Supplementary Figure S3A). To highlight the importance of individual residues for the interaction, we made a series of single mutations in Gp168 (Y14A, D21A, M25A and L30A) and checked their effects on the formation of the Gp168–clamp complex. As some mutants were highly prone to aggregation at high concentrations, size-exclusion chromatography coupled with SDS-PAGE was used to detect the complex. We found that Gp168^{Y14A} remained in the hexameric state (Supplementary Figure S4A) and lost the ability to form a complex

with β -clamp (Figure 4B), while Gp168^{D21A} retained the ability to form the β -clamp complex (Supplementary Figure S4B). Unfortunately, mutating M25 and L30 to alanine caused the recombinant proteins to appear to be in soluble under the same conditions (Supplementary Figure S4C). To determine their roles in complex formation, we made single mutations of the corresponding interacting residues on the β -clamp (namely, G285K, R283A and D336A). The abilities of β -clamp^{R283A} and β -clamp^{G285K} to form complexes with Gp168 were impaired (Figure 4C and D), while β -clamp^{D336A} did not disrupt the complex formation (Supplementary Figure S4D). Taken together, we determined the residues critical for the formation of the Gp168–clamp complex.

Gp168 interacts with *B. subtilis* β -clamp

Since β -clamp is highly conserved among bacteria, we proposed that Gp168 might interact with other bacterial clamps. First, we performed the sequence homology search using the loop-helix region sequence of β -clamp from different species, which was critical for the Gp168 binding (Figure 5A). Interestingly, these interface residues on β -clamp are highly conserved among many non-pathogenic bacteria like model organism *B. subtilis* and pathogenic *Bacilli* and *Clostridia*, including *Bacillus cereus*, *Bacillus anthracis*, *Clostridium botulinum* and *Clostridium tetani*. To test the hypothesis that Gp168 may interact with other β -clamps, we repeated the pull-down experiments using Gp168 and Gp168^{Y14A} with cell lysate of *B. subtilis*. Indeed, Gp168 co-eluted with β -clamp from the cell lysate (Figure 5B), but Gp168^{Y14A} failed to do so. No interaction was observed between Gp168^{Y14A} and β -clamp (Figure 5C) as the peak of Gp168^{Y14A} overlays with that of with β -clamp. Recombinant Gp168 expressed in *E. coli* did not co-elute with *E. coli* β -clamp or inhibit host growth (Figure 1A). Furthermore, Gp168 had no effect on *S. pyogenes* (16), which are consistent with the absence of conserved interacting residues in *E. coli* and *S. pyogenes* β -clamps (Figure 5A). Although we cannot test all bacterial β -clamps, our results suggest that Gp168 likely has an inhibitory effect against β -clamps from a range of pathogenic bacteria.

DISCUSSION

Bacteriophages are exclusive bacterial viruses that specialize in modifying host key enzymes. To initiate its own replication cycle, phages like T7 and SPO1 first hijack host RNA polymerase (RNAP) to start produce their own proteins, then produce RNAP inhibitors after its own RNAP is available (35–37). For example, *Xanthomonas oryzae* phage Xp10 produces protein P7 to inhibit host transcription initiation via the interaction between P7 and β' subunit of RNAP (38). And protein Ocr of *E. coli* phage T7 inhibits host transcription by competing with sigma factors for the recruitment of RNAP (39). To maximize the nucleotides pool for their own replication, phages like N4 and Twort also produce inhibitors that shutdown host DNA replication. β -clamp plays an important role in DNA replication and repair through its interaction with all DNA Pols

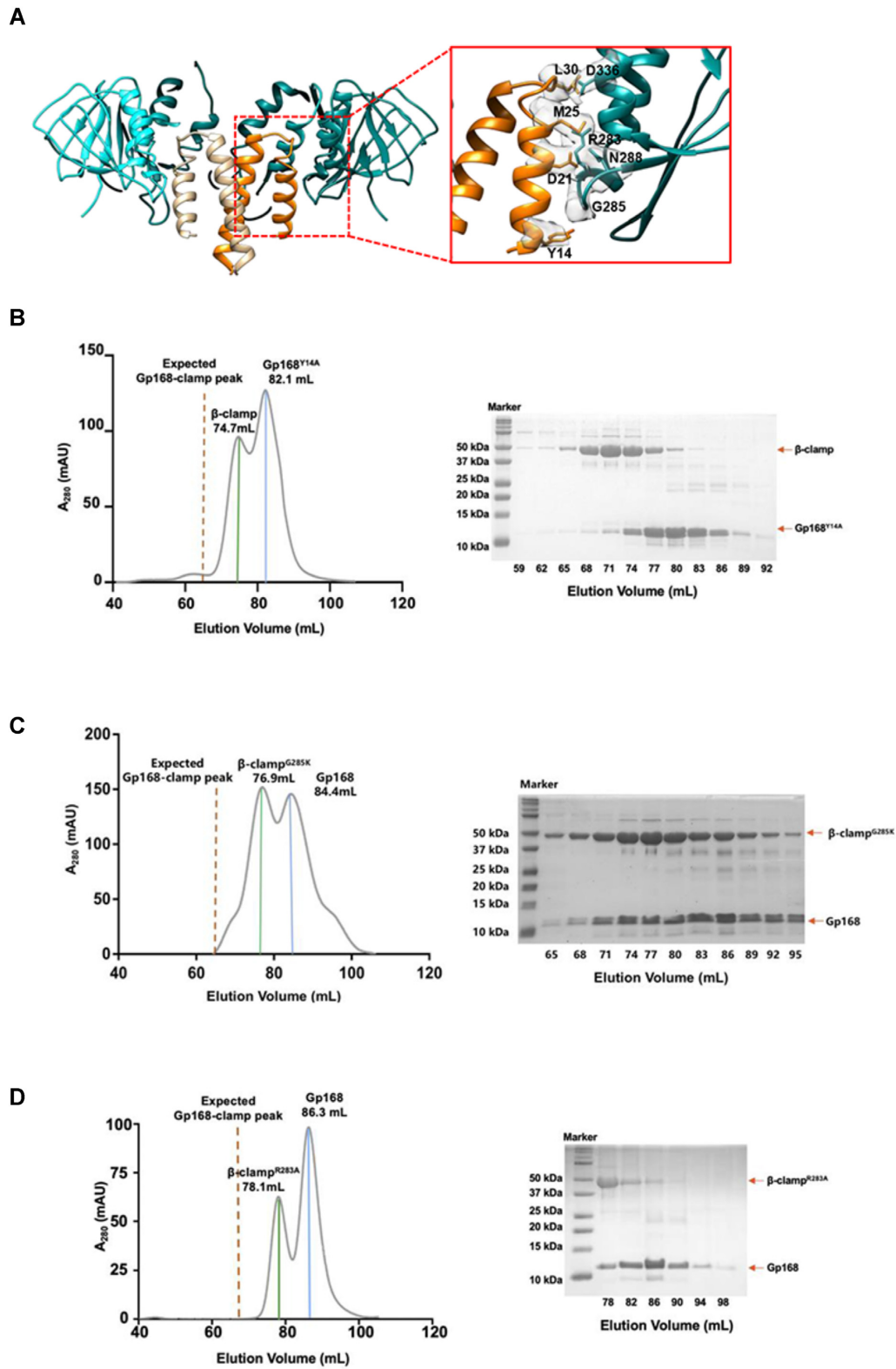


Figure 4. Pinpointing the residues critical for the Gp168-clamp complex formation. (A) Zoom-in map and model view of the representative interacting residues between Gp168 and β -clamp, demonstrating the good resolvability of involved residues. (B) Gel filtration chromatographic profiles of β -clamp and Gp168^{Y14A} mixture, and SDS-PAGE of the corresponding fractions. (C) Gel filtration chromatographic profiles of the mixture of β -clamp^{G285K} and Gp168, and SDS-PAGE of the corresponding fractions. (D) Gel filtration chromatographic profiles of the mixture of β -clamp^{R283A} and Gp168, and SDS-PAGE of the corresponding fractions.

A

		Helix		Loop			
<i>S. aureus</i>	331	S	KYMMDALKA	340	275	IDRASLLAREGGNNV	289
<i>B. subtilis</i>	332	P	KYMLDALKV	341	275	IDRASLLAREGRNNV	289
<i>B. cereus</i>	335	A	KYMMDALKA	344	278	IDRASLLARDGRNNV	292
<i>B. anthracis</i>	333	A	KYMMDALKA	342	276	IDRASLLARDGRNNV	290
<i>C. botulinum</i>	319	S	KYLLDVLKT	328	265	IERASLMAKEGNTNL	279
<i>C. tetani</i>	319	S	KYLIDVLKV	328	265	IERASLMGKDNTSL	279
<i>S. pyogenes</i>	331	P	TYLIESLKA	340	275	MERAFLLISNATQNGT	289
<i>E. coli</i>	321	V	SYVLDVLSNA	330	267	FARAAILSNEKFRGV	281

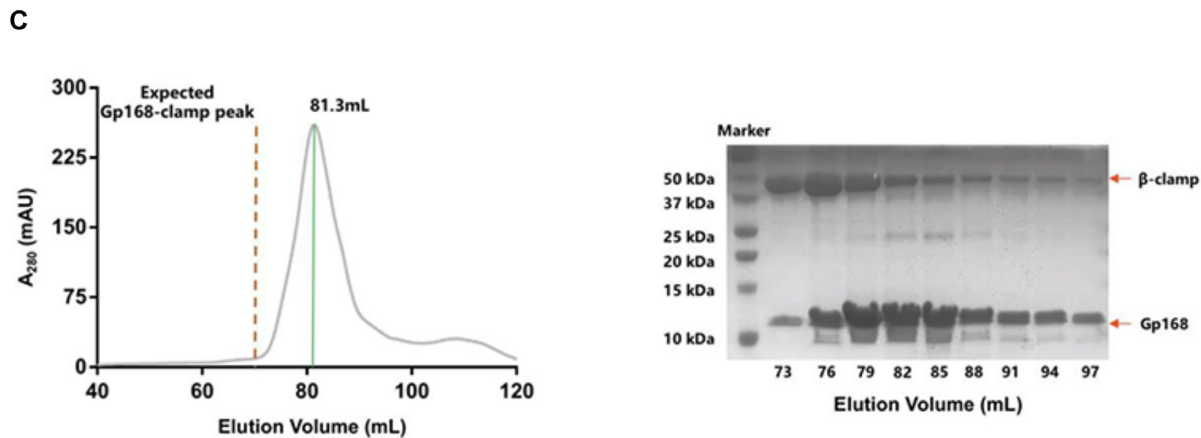
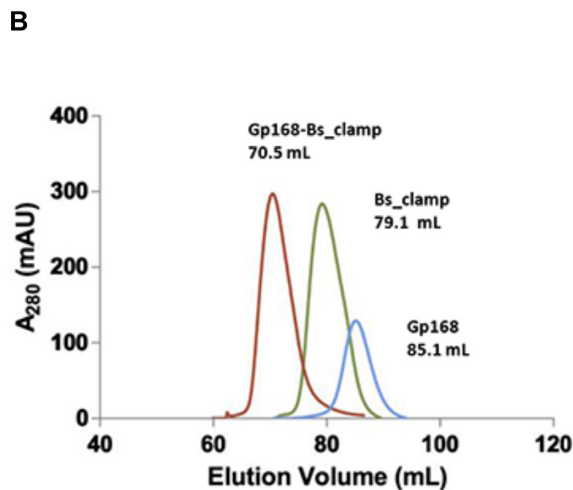


Figure 5. The potential cross-species inhibitory effect of Gp168. (A) Multi-sequence alignment using corresponding sequences of *S. aureus*, *B. subtilis*, *B. cereus*, *B. anthracis*, *C. botulinum*, *C. tetani*, *E. coli* and *S. pyogenes* was performed by Clustal Omega. (B) Gel filtration chromatographic profiles of recombinantly expressed *B. subtilis* β-clamp (green), Gp168 (blue), and co-eluted Gp168-clamp complex (brown). The chromatography was performed using a Hiload Superdex 200 column. (C) Gel filtration chromatographic profile of *B. subtilis* β-clamp and Gp168^{Y14A} mixture. The SDS-PAGE image shows the elution volumes of the two proteins are both at around 81.3 ml.

and other factors and is therefore indispensable for bacteria. Most β -clamp binding proteins use the same protein-binding surface which overlaps with the clamp loader binding site, thereby avoiding removal of β -clamp by the clamp loader while these enzymes are at work on DNA. Two phage proteins (Gp168 and Gp240) have been described as potent β -clamp inhibitors with the ability to inhibit both the clamp loading step and processive DNA replication. Using a stepwise reconstitution of processive DNA replication *in vitro*, the phage proteins were postulated to interact with the protein-binding surface and compete with DNA Pol and clamp loader (16). In our study, we demonstrate that Gp168 disassembly from a hexamer precedes the Gp168/ β -clamp interaction where it interacts as a dimer. Importantly, the binding affinity of Gp168/ β -clamp interaction (95 nM) is stronger than that between β -clamp of *E. coli* and primed-DNA (120 nM) or blunt DNA duplex (453 nM) (14). It is also useful to note that Gp168/ β -clamp interaction based on our measured apparent affinity is significantly weaker than that between the β -clamp and clamp loader complex (3 nM in the presence of MgCl₂ and ATP) (40). As the Gp168/ β -clamp interaction includes two events: depolymerization of hexameric Gp168 and complex formation between depolymerized Gp168 and β -clamp, the ITC experiment recorded the overall heat signature instead of that of the second step. As the depolymerization of Gp168 is endothermic (Supplementary Figure S5) and the Gp168-clamp interaction reaction is overall an exothermic reaction, the overall heat recorded in ITC is reduced due to the endothermic disassembly step. Consequently, the affinity calculated is weaker than the real affinity for complex formation from monomeric Gp168. We therefore term our calculated affinity as an ‘apparent’ affinity as it is an estimate of the lower limit. Thus, our measured apparent affinity can be used to compare with interactions with lower affinities, i.e. β -clamp/DNA interaction, but not with interactions with higher affinities as the degree of the underestimation is not clear. Similarly, the stoichiometry ($N = 0.16 \pm 0.003$) derived from ITC should not be attributed to the second step.

The cryo-EM structure of the Gp168-clamp complex at the 3.2-Å resolution reveals that Gp168 occupies the DNA sliding circle of β -clamp, instead of engaging the protein-binding pocket located between domain II and III. Using this strategy, Gp168 is not in a direct competition with the high affinity clamp loader complex at the hydrophobic pocket, and its affinity for the β -clamp can be independently fine-tuned such that it is higher than that of the β -clamp/primed-DNA or blunt DNA duplex complexes. The Gp168 complex would predominate when β -clamp is transferred to primed DNA and therefore block loading. Gp168 utilises a distinct set of residues located at the inner circle of the β -clamp when compared to the DNA complex, of which Y14_{Gp168} with G285_{clamp} represents a key interaction. The conservation of these residues suggest that Gp168 is potentially a cross-species β -clamp inhibitor.

DNA clamps are fundamental for living organisms and have therefore been explored for antibacterial and anti-tumor purposes, respectively. For antibacterial studies, various β -clamp inhibitors including peptide-based inhibitors, small molecule inhibitors, and natural compounds have

been investigated to a great extent (41). Not surprisingly, all of these inhibitors compete with β -clamp interacting proteins. In contrast, Gp168 utilises an alternative interaction surface that could be explored in the search for new inhibitors. The small size of Gp168, and even smaller Gp240, suggest that peptide-based mimetics would be suitable for designing inhibitors that target this interface. Peptide-based therapeutic have been shown effective in treating bacterial infection in animal tests (42), Gp168 inspired peptides could be considered for such application. In summary, our study not only provides new insight into how bacteriophages target DNA clamps but could provide inspiration for the development of new antimicrobial reagents.

DATA DEPOSITION

Cryo-EM map of the Gp168-clamp complex in this study with its associated atomic model have been deposited in the wwPDB OneDep System under EMD accession code EMD-31339 and PDB ID code 7EVP, respectively.

SUPPLEMENTARY DATA

Supplementary Data are available at NAR Online.

ACKNOWLEDGEMENTS

We are grateful for the help from the National Facility for Protein Science, Shanghai Advanced Research Institute with cryo-EM sample evaluation, and instrument analysis center of Xi’an Jiaotong University for grid screening and the High-End Cryo-EM Platform, Core Facility Center for Life Sciences at University of Science and Technology of China for data collection.

Author contributions: B.L. and K.Z. conceived the project and designed the experiments. B.L., Y.L. and H.C. purified the proteins, assembled the complex, and made mutation constructs. Z.H. and H.W. performed the functional assays. Z.W. purified Gp168 and determined the multimeric state. B.M. carried out the NMR experiments. Y.Z. and L.Z. performed initial screening for cryo-EM. S.L. and K.Z. performed cryo-EM experiments and solved the complex structure. B.L., S.L. and K.Z. analyzed the data. B.L. wrote the first draft of the manuscript. B.L., S.L., S.M. and K.Z. revised the manuscript with contributions from all authors.

FUNDING

Key research and development plan of Shaanxi Province [2021ZDLSF01-10]; National Natural Science Foundation of China [81871662]; Start-up funding from University of Science and Technology of China [KY910000032, KJ2070000080].

Conflict of interest statement. None declared.

REFERENCES

- O'Donnell, M., Langston, L. and Stillman, B. (2013) Principles and concepts of DNA replication in bacteria, archaea, and eukarya. *Cold Spring Harb. Perspect. Biol.*, **5**, a010108.
- Kong, X.P., Onrust, R., O'Donnell, M. and Kuriyan, J. (1992) Three-dimensional structure of the beta subunit of *E. coli* DNA polymerase III holoenzyme: a sliding DNA clamp. *Cell*, **69**, 425–437.

3. Kazmirski, S.L., Podobnik, M., Weitze, T.F., O'Donnell, M. and Kuriyan, J. (2004) Structural analysis of the inactive state of the *Escherichia coli* DNA polymerase clamp-loader complex. *Proc. Natl. Acad. Sci. U.S.A.*, **101**, 16750–16755.
4. Jeruzalmi, D., O'Donnell, M. and Kuriyan, J. (2001) Crystal structure of the processivity clamp loader gamma (gamma) complex of *E. coli* DNA polymerase III. *Cell*, **106**, 429–441.
5. Onrust, R., Finkelstein, J., Turner, J., Naktinis, V. and O'Donnell, M. (1995) Assembly of a chromosomal replication machine - 2 DNA-polymerases, a clamp loader, and sliding clamps in one holoenzyme particle. 3. Interface between two polymerases and the clamp loader. *J. Biol. Chem.*, **270**, 13366–13377.
6. Stukenberg, P.T., Studwellvaughan, P.S. and O'Donnell, M. (1991) Mechanism of the sliding beta-clamp of DNA polymerase-III holoenzyme. *J. Biol. Chem.*, **266**, 11328–11334.
7. Krishna, T.S., Kong, X.P., Gary, S., Burgers, P.M. and Kuriyan, J. (1994) Crystal structure of the eukaryotic DNA polymerase processivity factor PCNA. *Cell*, **79**, 1233–1243.
8. Moarefi, I., Jeruzalmi, D., Turner, J., O'Donnell, M. and Kuriyan, J. (2000) Crystal structure of the DNA polymerase processivity factor of T4 bacteriophage. *J. Mol. Biol.*, **296**, 1215–1223.
9. Matsumiya, S., Ishino, Y. and Morikawa, K. (2001) Crystal structure of an archaeal DNA sliding clamp: proliferating cell nuclear antigen from *Pyrococcus furiosus*. *Protein Sci.*, **10**, 17–23.
10. Kelman, Z. and O'Donnell, M. (1995) Structural and functional similarities of prokaryotic and eukaryotic DNA-polymerase sliding clamps. *Nucleic Acids Res.*, **23**, 3613–3620.
11. O'Donnell, M., Jeruzalmi, D. and Kuriyan, J. (2001) Clamp loader structure predicts the architecture of DNA polymerase III holoenzyme and RFC. *Curr. Biol.*, **11**, R935–946.
12. Lopez de Saro, F.J. and O'Donnell, M. (2001) Interaction of the beta sliding clamp with MutS, ligase, and DNA polymerase I. *Proc. Natl. Acad. Sci. U.S.A.*, **98**, 8376–8380.
13. Kurz, M., Dalrymple, B., Wijffels, G. and Kongsuwan, K. (2004) Interaction of the sliding clamp beta-subunit and Hda, a DnaA-related protein. *J. Bacteriol.*, **186**, 3508–3515.
14. Georgescu, R.E., Kim, S.S., Yurieva, O., Kuriyan, J., Kong, X.P. and O'Donnell, M. (2008) Structure of a sliding clamp on DNA. *Cell*, **132**, 43–54.
15. Liu, J., Dehbi, M., Moeck, G., Arhin, F., Bauda, P., Bergeron, D., Callejo, M., Ferretti, V., Ha, N.H., Kwan, T. *et al.* (2004) Antimicrobial drug discovery through bacteriophage genomics. *Nat. Biotechnol.*, **22**, 185–191.
16. Bellej, A., Callejo, M., Arhin, F., Dehbi, M., Fadhil, I., Liu, J., McKay, G., Srikumar, R., Bauda, P., Bergeron, D. *et al.* (2006) Competition of bacteriophage polypeptides with native replicase proteins for binding to the DNA sliding clamp reveals a novel mechanism for DNA replication arrest in *Staphylococcus aureus*. *Mol. Microbiol.*, **62**, 1132–1143.
17. Scheres, S.H. (2012) RELION: implementation of a Bayesian approach to cryo-EM structure determination. *J. Struct. Biol.*, **180**, 519–530.
18. Zheng, S.Q., Palovcak, E., Armache, J.P., Verba, K.A., Cheng, Y. and Agard, D.A. (2017) MotionCor2: anisotropic correction of beam-induced motion for improved cryo-electron microscopy. *Nat. Methods*, **14**, 331–332.
19. Rohou, A. and Grigorieff, N. (2015) CTFFIND4: Fast and accurate defocus estimation from electron micrographs. *J. Struct. Biol.*, **192**, 216–221.
20. Punjani, A., Rubinstein, J.L., Fleet, D.J. and Brubaker, M.A. (2017) cryoSPARC: algorithms for rapid unsupervised cryo-EM structure determination. *Nat. Methods*, **14**, 290–296.
21. Pettersen, E.F., Goddard, T.D., Huang, C.C., Couch, G.S., Greenblatt, D.M., Meng, E.C. and Ferrin, T.E. (2004) UCSF Chimera – a visualization system for exploratory research and analysis. *J. Comput. Chem.*, **25**, 1605–1612.
22. Pintilie, G.D., Zhang, J., Goddard, T.D., Chiu, W. and Gossard, D.C. (2010) Quantitative analysis of cryo-EM density map segmentation by watershed and scale-space filtering, and fitting of structures by alignment to regions. *J. Struct. Biol.*, **170**, 427–438.
23. Adams, P.D., Afonine, P.V., Bunkoczi, G., Chen, V.B., Davis, I.W., Echols, N., Headd, J.J., Hung, L.W., Kapral, G.J., Grosse-Kunstleve, R.W. *et al.* (2010) PHENIX: a comprehensive Python-based system for macromolecular structure solution. *Acta Crystallogr. D. Biol. Crystallogr.*, **66**, 213–221.
24. Emsley, P., Lohkamp, B., Scott, W.G. and Cowtan, K. (2010) Features and development of Coot. *Acta Crystallogr. D. Biol. Crystallogr.*, **66**, 486–501.
25. Terwilliger, T.C., Adams, P.D., Afonine, P.V. and Sobolev, O.V. (2018) A fully automatic method yielding initial models from high-resolution cryo-electron microscopy maps. *Nat. Methods*, **15**, 905–908.
26. Chen, V.B., Arendall, W.B. 3rd, Headd, J.J., Keedy, D.A., Immormino, R.M., Kapral, G.J., Murray, L.W., Richardson, J.S. and Richardson, D.C. (2010) MolProbity: all-atom structure validation for macromolecular crystallography. *Acta Crystallogr. D. Biol. Crystallogr.*, **66**, 12–21.
27. Pintilie, G., Zhang, K., Su, Z., Li, S., Schmid, M.F. and Chiu, W. (2020) Measurement of atom resolvability in cryo-EM maps with Q-scores. *Nat. Methods*, **17**, 328–334.
28. Laskowski, R.A., Jablonska, J., Pravda, L., Varkova, R.S. and Immormino, J.M. (2018) PDBsum: Structural summaries of PDB entries. *Protein Sci.*, **27**, 129–134.
29. Lopez de Saro, F.J. (2009) Regulation of interactions with sliding clamps during DNA replication and repair. *Curr. Genomics*, **10**, 206–215.
30. Almawi, A.W., Scotland, M.K., Randall, J.R., Liu, L.D., Martin, H.K., Sacre, L., Shen, Y., Pillon, M.C., Simmons, L.A., Sutton, M.D. *et al.* (2019) Binding of the regulatory domain of MutL to the sliding beta-clamp is species specific. *Nucleic Acids Res.*, **47**, 4831–4842.
31. Waterhouse, A., Bertoni, M., Bienert, S., Studer, G., Tauriello, G., Gumienny, R., Heer, F.T., de Beer, T.A.P., Rempfer, C., Bordoli, L. *et al.* (2018) SWISS-MODEL: homology modelling of protein structures and complexes. *Nucleic Acids Res.*, **46**, W296–W303.
32. Boratyn, G.M., Thierry-Mieg, J., Thierry-Mieg, D., Busby, B. and Madden, T.L. (2019) Magic-BLAST, an accurate RNA-seq aligner for long and short reads. *BMC Bioinformatics*, **20**, 405.
33. Holm, L. (2020) DALI and the persistence of protein shape. *Protein Sci.*, **29**, 128–140.
34. Boyken, S.E., Chen, Z., Groves, B., Langan, R.A., Oberdorfer, G., Ford, A., Gilmore, J.M., Xu, C., DiMaio, F., Pereira, J.H. *et al.* (2016) De novo design of protein homo-oligomers with modular hydrogen-bond network-mediated specificity. *Science*, **352**, 680–687.
35. James, E., Liu, M.H., Sheppard, C., Mekler, V., Camara, B., Liu, B., Simpson, P., Cota, E., Severinov, K., Matthews, S. *et al.* (2012) Structural and mechanistic basis for the inhibition of *Escherichia coli* RNA polymerase by T7 Gp2. *Mol. Cell*, **47**, 755–766.
36. Tabib-Salazar, A., Liu, B., Barker, D., Burchell, L., Qimron, U., Matthews, S.J. and Wigneshweraraj, S. (2018) T7 phage factor required for managing RpoS in *Escherichia coli*. *Proc. Natl. Acad. Sci. U.S.A.*, **115**, E5353–E5362.
37. Wang, Z.H., Wang, H.L., Mulvanna, N., Sanz-Hernandez, M., Zhang, P.P., Li, Y.Q., Ma, J., Wang, Y.W., Matthews, S., Wigneshweraraj, S. *et al.* (2021) A bacteriophage DNA mimic protein employs a non-specific strategy to inhibit the bacterial RNA polymerase. *Front Microbiol.*, **12**, 692512.
38. Liu, B., Shadrin, A., Sheppard, C., Mekler, V., Xu, Y.Q., Severinov, K., Matthews, S. and Wigneshweraraj, S. (2014) A bacteriophage transcription regulator inhibits bacterial transcription initiation by Sigma-factor displacement. *Nucleic Acids Res.*, **42**, 4294–4305.
39. Ye, F.Z., Kotta-Loizou, I., Jovanovic, M., Liu, X.J., Dryden, D.T.F., Buck, M. and Zhang, X.D. (2020) Structural basis of transcription inhibition by the DNA mimic protein Ocr of bacteriophage T7. *Elife*, **9**, e52125.
40. Naktinis, V., Onrust, R., Fang, L.H. and O'Donnell, M. (1995) Assembly of a chromosomal replication machine - 2 DNA-polymerases, a clamp loader, and sliding clamps in one holoenzyme particle. 2. Intermediate complex between the clamp loader and its clamp. *J. Biol. Chem.*, **270**, 13358–13365.
41. Altieri, A.S. and Kelman, Z. (2018) DNA sliding clamps as therapeutic targets. *Front Mol Biosci*, **5**, 00087.
42. Nedal, A., Raeder, S.B., Dalhus, B., Helgesen, E., Forstrom, R.J., Lindland, K., Sumabe, B.K., Martinsen, J.H., Kragelund, B.B., Skarstad, K. *et al.* (2020) Peptides containing the PCNA interacting motif APIM bind to the beta-clamp and inhibit bacterial growth and mutagenesis. *Nucleic Acids Res.*, **48**, 5540–5554.